Superparamagnetic $NiFe_2O_4$ Nanoparticles to Remove Arsenic From Drinking Water

Yüksel Köseoğlu
Fatih University, Department of Physics, Buyukcekmece 34500 Istanbul-TURKEY

Abstract: Superparamagnetic nanoparticles of nickel ferrite ($NiFe_2O_4$) were produced by PEG assisted hydrothermal method. XRD, FT-IR, TEM and VSM were used for the structural, morphological, and magnetic investigation of the product, respectively. Average particle size of the nanoparticles was estimated by the Scherrer equation using the full-width at half maximum (FWHM) of the most intense XRD peak and found as 14 nm. While the nanoparticles indicate a superparamagnetic behavior above the blocking temperature of 72 K, they have ferromagnetic behavior at temperatures lower than the blocking temperature. These nanoparticles were dispersed into drinking water contaminated with arsenic (As), and once they bind to arsenic, they have been removed from the water solution using a strong magnet. The results were measured by Atomic Mass Spectrometry and found that these nanoparticles had removed 90 % of the arsenic. The measurements were repeated several times with the same sample and get almost the same results.

Keywords: Superparamagnetism, Ferrite, XRD, VSM, Atomic mass spectroscopy, Arsenic

Introduction

Nanophase materials with an average grain size in the range of 1 to 50 nm have attracted research interest for more than a decade since their physical properties are quite different from that of their bulk micron-sized counterparts because of the large volume fraction of atoms that occupies the grain boundary area [1-3]. This new class of materials is used in important applications like high frequency transformers, ferrofluids, pigments in paints and ceramics, biomedical applications like drug delivery system, hyperthermia, NMR, high density magnetic recording, varistors and dye-sensitized solar cells [4-11]. The surface area of the nanostructured materials is large as the grain sizes are small. The increase in the interfacial energy due to defects, dislocations and lattice imperfections leads to changes in various physical properties and hence one can tailor make the materials with specific properties. Almost 50 % of the atoms reside in the grain boundary area when the grain size is reduced to less than 10 nm whereas it is only 1-3 % when the grain size is 100 nm [1, 12]. Since a large fraction of atoms is present at the grain boundaries, the nanocrystalline materials exhibit enhanced diffusivity.

Arsenic (As) contamination in drinking water is a major health and environmental issue around the world, especially in the developing countries [13,14]. Removal of arsenic from drinking water is an important problem for environmental engineering and while there are ways to remove arsenic, thay are expensive and require extensive hardware and high-pressure pumps that run on electricity. Iron oxide is an interesting sorbent for the removal of arsenic and other heavy metal contaminants[15,16]. When magnetic iron oxide is made as nanoparticles, the smaller particle size and high surface area enhances its capacity for As removal [17]. An external magnetic field can be used to separate the magnetic nanoparticles after sorption.

Here we report the PEG assisted hydrothermal synthesis of nickel ferrite ($NiFe_2O_4$) nanoparticles and show the potential use of the nanocomposite of superparamagnetic $NiFe_2O_4$ for the waste water treatment, especially for arsenic removal, by magnetic separation, using a small magnetic field. The experiments involved suspending pure samples of uniform-sized nickel ferrite nanoparticles in water. Once they bind to arsenic, a magnetic field was used to pull the particles to out of solution, leaving only the purified water. We measured the tiny particles after they were removed from the water and ruled out the most obvious explanation: the particles were not clumping together after being tractored by the magnetic field due to surface modification by polyethylene glycol (PEG). It is also found that the composite can be easily dispersed in water and the magnetic carbon fluid thus obtained is very stable for few days.

Results and Discussion

FTIR analysis

Two mainbroad metal-oxygen bands are seen in the IR spectra of all spinels, and ferrites in particular. The highest one, v_1, (Fig. 1) generally observed in the range 600-550cm^{-1}, corresponds to intrinsic stretching vibrations of the metal at the tetrahedral site, $M_{tetra}\leftrightarrow O$, whereas the v_2-lowest band, usually observed in the range 450-385cm^{-1}, is assigned to octahedral-metal stretching, $M_{octa}\leftrightarrow O$ [7,18]. It is known that Ni^{2+} ions have octahedral-site preference Fe^{2+} and Fe^{3+} ions can occupy both octahedral and tetrahedral sites [19].

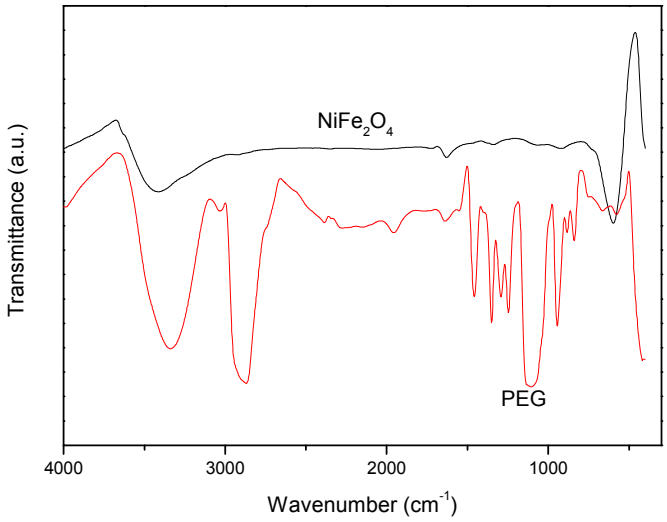

Fig. 1. FTIR spectra of $NiFe_2O_4$, synthesized by PEG-assisted hydrothermal method. Red line shows the FTIR spectra of PEG.

However, no clear peak due to octahedrally coordinated metal ions has been observed which is expected to be below 400 cm^{-1}. This may be due to the broadening of this peak attributed to very small particles of spinel ferrites. The bands observed around 3430 and 1521 cm^{-1} frequencies are ascribed due to the stretching modes and H-O-H bending vibration of the free or absorbed water molecules.

XRD analysis

The powder X-ray diffractograms recorded for sample of $NiFe_2O_4$ nanoparticles is shown in Fig.2. Samples are considered to be single-phase spinel structure as no extra peaks and no unreacted constituents were observed. This allows the estimation of average crystallite size and its standart deviation from XRD. The experimental line profiles, shown in Fig.2, were fitted for 9 peaks (111), (220), (311), (400), (422), (511), (440) (622) and (533) the calculated average crystallite size, D and standart deviations σ, are presented in Table 3.

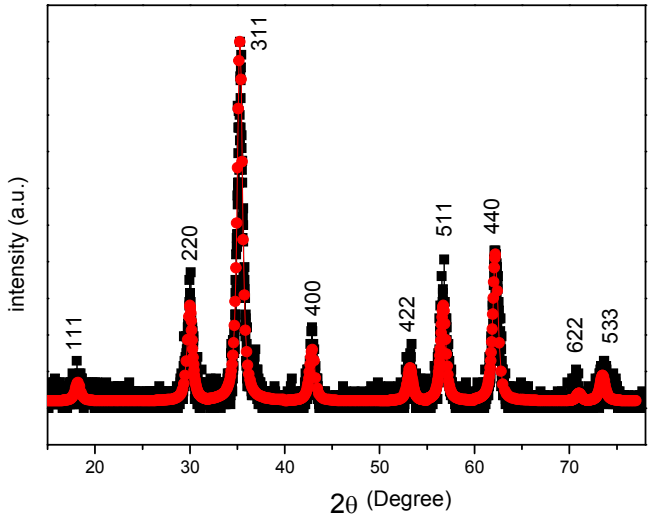

Figure 2: Experimental and theoretically fitted XRD patterns of $NiFe_2O_4$ nanoparticles.

The cation distribution in $NiFe_2O_4$ can be infered from the X-ray diffraction relative integrated intensity calculations by using the following formula suggested by Buerger [20]:

$$I_{hkl} = |F|^2_{hkl} PL_p \qquad (1)$$

where F is the structure factor, P the multicipty factor and L_p is the Lorenz-polarization factor which depends only on the Bragg's diffraction angle θ

$$L_p = \frac{1+\cos^2 2\theta}{\sin^2\theta\cos 2\theta} \qquad (2)$$

Some peaks' intensity ratios in the XRD pattern of spinel structures were reported as cation distribution sensitive peaks, such as I_{220}/I_{400}, I_{220}/I_{422} and I_{422}/I_{400} [21,22]. In the calculations (i) all possible cation arrangments are considered with 0.01 stoichiometric sensitivity that Ni^{+2} and Fe^{+3} can site both tetrahedral and octahedral sites, (ii) the oxygen positional parameter was chosen between 0.3700 and 0.3900, ideal spinel structures that are 0.3852, 0.3822 and 0.375 respectively [23] and (iii) for the agreement of calculated and experimental intensity ratios, the difference of calculated and experimental relative intensities for all distribution cases are considered and the sum of these differences are minimized. Finally the closest calculated data are taken to be the correct distributions. Note that there should be no need for the thermal correction because of the spinel's high melting temperature and hence very small thermo-vibrational effect of spinel on XRD patterns [24]. As a result the experimental lattice constants, chosen oxygen positional parameters, the relative insenties of experimental and calculated XRD peaks, and their corresponding cation distribution results are listed in Table 1. The occupancy of Fe^{+3} ions on A site is greater than 0.78 and in all substance the Fe^{+3} ions dominate in T_d sub lattice.

Lattice Parameter a (A)	Oxygen Positional Parameter u	Cation Distribution	I_{220}/I_{400}		I_{422}/I_{400}	
			Obs.	Cal.	Obs.	Cal.
8.36	0.3750	$(Ni_{0.22}Fe_{0.78})$ $[Ni_{0.78}Fe_{1.22}]$	1.25	1.23	0.41	0.45

Table 1: The values of XRD cation distribution in $NiFe_2O_4$ nanoparticles.

In the spinel structure the cations on different sub lattites (A and B sites) have oppositely aligned magnetic moments according to the Neel's ferrimagnetic theory [55]. So the magnetic moment per formula unit in μ_B (Bohr magneton) is

$$n_B(x) = M_B(x) - M_A(x) \qquad (4.4)$$

where M_B and M_A are B and A site magnetic moment in μ_B. The magnetic moment per formula unit is calculated by cation distribution results of XRD and Neel's theory with ionic magnetic moment of 5 μ_B and 2 μ_B for Fe^{+3} and Ni^{+2}, respectively [23]. The results are summarized in Table 2. The calculated n_B values agreed well with experimentally obtained values, confirming a collinear magnetic structure.

.

Cation Distribution (XRD)	Saturation Magnetization Ms (emu/g) (VSM)	Magneton number $n_B(\mu_B)$	
		Obs. (VSM)	Cal. (XRD)
$(Ni_{0.22}Fe_{0.78})$ $[Ni_{0.78}Fe_{1.22}]$	40.93	2.16	2.20

Table 2: The magnetic moment per unit formula from XRD and VSM for $NiFe_2O_4$ nanoparticles

TEM	(XRD- Profile Fit)	VSM (LN Langevien Fit)
D_{TEM} (σ) Av. Size (Geo.StD)	D_{XRD} (σ) Av. Size (StD.)	$D_m(\sigma_m)$ Av. Size (Geo .StD.)
15 (0.23)	14.1 (5.0)	13.9 (0.58)

Table 3: The obtained particle sizes or size distributions of Ni Fe_2O_4 nanoparticles.

TEM analysis

The TEM micrograph and particle size distribution of $NiFe_2O_4$ nanoparticles synthesized by by hydrothermal method using PEG 400 are given in Fig. 3. During synthesis, temperature was increased to 150 ^{0}C and samples were kept for 21h in the owen. A good crystallinity can be attributed to the heat during synthesis process. 150 particles are counted in $NiFe_2O_4$ nanoparticles and particle size has been determined as 15 nm from the size distribution from Fig.3 (b) which agrees with the result of XRD measurement (14.1 nm).

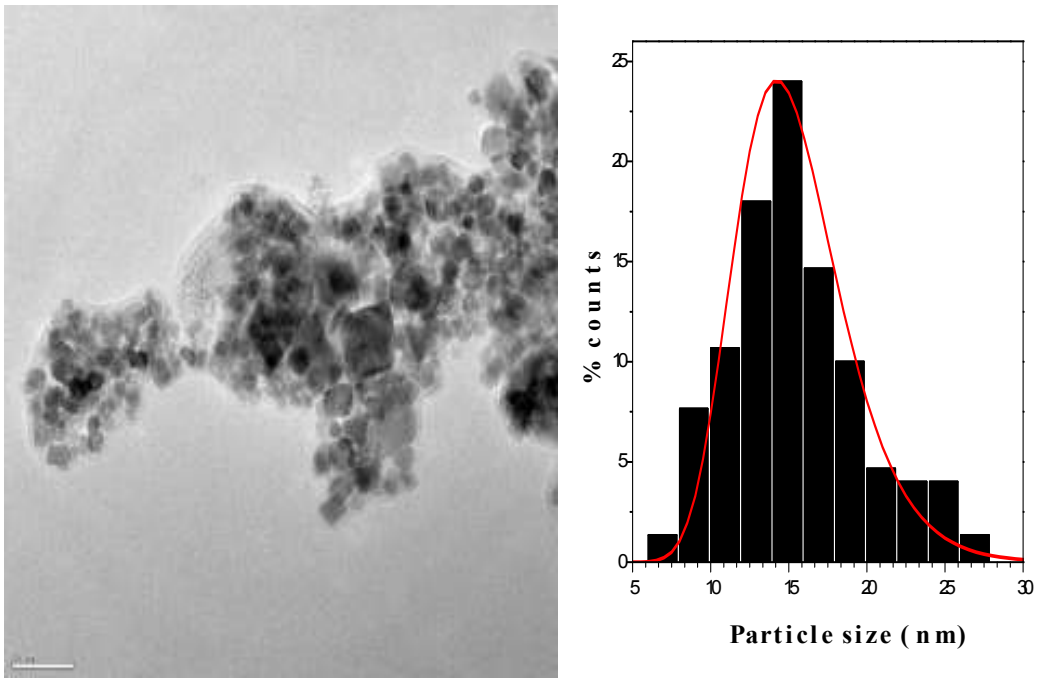

(a) **(b)**

Figure 3 (a) The TEM micrograph of $NiFe_2O_4$ nanoparticles synthesized by using PEG 400, **(b)** particle size distribution.

VSM analysis

By using Quantum Design Vibrating Sample Magnetometer (QD-VSM), the magnetic characterizations of $NiFe_2O_4$ nanoparticles were performed. In detail, the magnetization of Ni-ferrites were studied as a function of external field between ±5 kOe and as a function of temperature (between T=10 K and the room temperature). Magnetic hysteresis curves were then analyzed for temperature dependency of the samples' magnetization under zero field cooling-ZFC and field cooling-FC.

The magnetization curve of $NiFe_2O_4$ nanoparticles synthesized by hydrothermal method using PEG 400 is analized at room and 10 K temperature in Fig. 4 and 5.

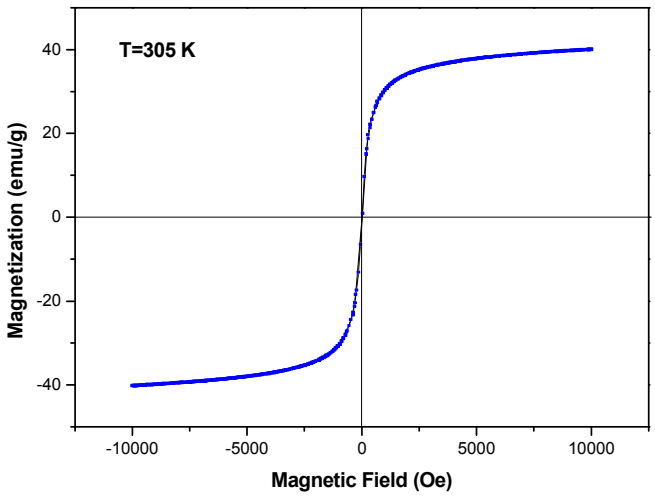

Figure 4 Magnetic field vs magnetization curve of $NiFe_2O_4$ synthesized by hydrothermal method using PEG 400 at room temperature.

It is observed that the room temperature M-H curve of $NiFe_2O_4$ powders does not show a hysteresis in Fig. 4. The value of magnetization sharply increases with the external magnetic field strength. M-H curve has an s shape at low field region and the high field side of the curve is almost linear with the external field. However, a saturation state of magnetization has not been reeached yet in the presence of a relatively strong magnetic field of even 10 kOe, which is consistent with the previous studies [25,26]. A saturation magnetization of 40.93 emu/g is obtained for the room temperature measurement.

It is known that fine particles are easy to activate thermally and overcome magnetic anisotropy. Particles lost their hysteresis property above blocking temperature and magnetic moments follow the same direction with applied magnetic field. So that the magnetic moments do not have any remanent magnetization and a hysteresis loop to observe coercive field.

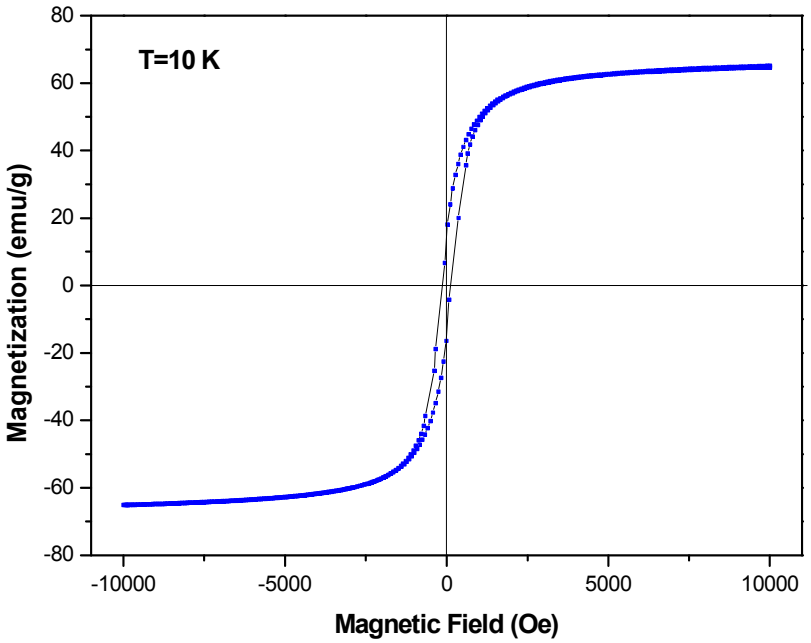

Figure 5 Magnetic field vs magnetization curve of $NiFe_2O_4$ synthesized by hydrothermal method using PEG 400 as fuel at 10K temperature.

The M-H curve of $NiFe_2O_4$ nanoparticles denoted that coercive field and saturation magnetization increased at 10 K temperature in Fig. 5. Coercive field is measured as 132 Oe which is higher than 305K value. And saturation magnetization reached 65.35 emu/g because of the magnetic exchange energy. The width of hysteresis terminates around 50 emu/g values, after that a line follows a continuous shape by increasing applied field. An increasing trend in saturation magnetization is also observed in the high magnetic field regime.

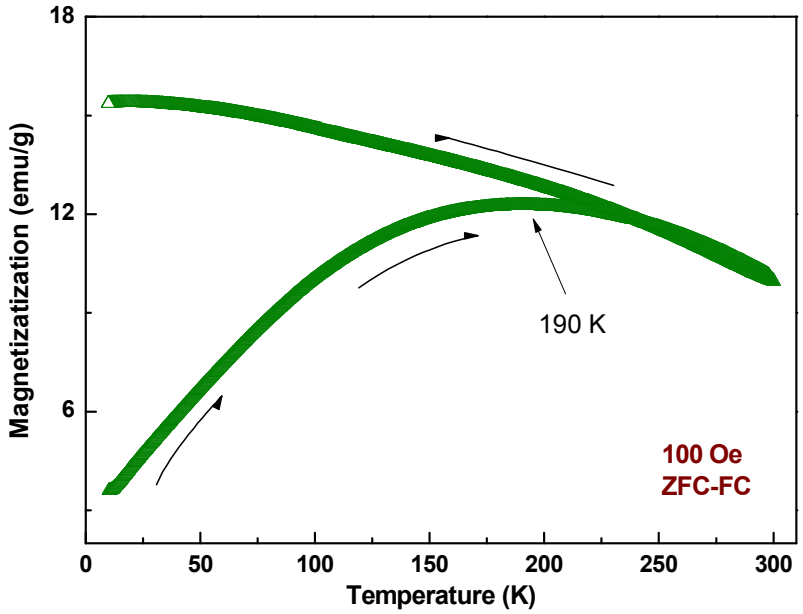

Figure 6 Magnetization vs temperature curve of $NiFe_2O_4$ synthesized by hydrothermal method using PEG 400 as fuel.

The magnetization vs temperature curve of $NiFe_2O_4$ synthesized by hydrothermal method using PEG 400 as fuel has been obtained in Fig. 6. The magnetization of the $NiFe_2O_4$ sample increases by decreasing temperature in FC (field cooling) measurement. The magnetization of $NiFe_2O_4$ nanoparticles at 10 K temperature is measured as 15 emu/g in FC process which means the magnetization direction of each particle is frozen in the field direction. The ZFC magnetization exhibits a maximum around a critical temperature which is blocking temperature T_B. Both curves, only joins at around 220 K temperature only and then diverges. Here, the blocking temperature (T_B) of $NiFe_2O_4$ nanoparticles is determined as 190 K as seen in Fig. 6. After ZFC process, magnetization of $NiFe_2O_4$ nanoparticles is measured as 4 emu/g which denotes that the magnetic moments did not align at 10 K temperature.

Arsenic Removal

The $NiFe_2O_4$ nanoparticles covered with PEG can be easily dispersed in water and the dispersion is found to be stable for a long time. Similarly, the nanocomposite can be easily separated using a laboratory permanent magnet and again redispersed. This shows that the PEG is strongly attached to the surface of the Ni-ferrite nanoparticles. To demonstrate the application of the Ni-ferrite nanocomposite for arsenic removal by magnetic separation, the nanocomposite is used for the removal of arsenic in drinking water. The photographs in Figure 7 (a) show this behavior very clearly. This shows the efficiency of the nanocomposite for arsenic removal after adsorption on nickel ferrite by magnetic separation.

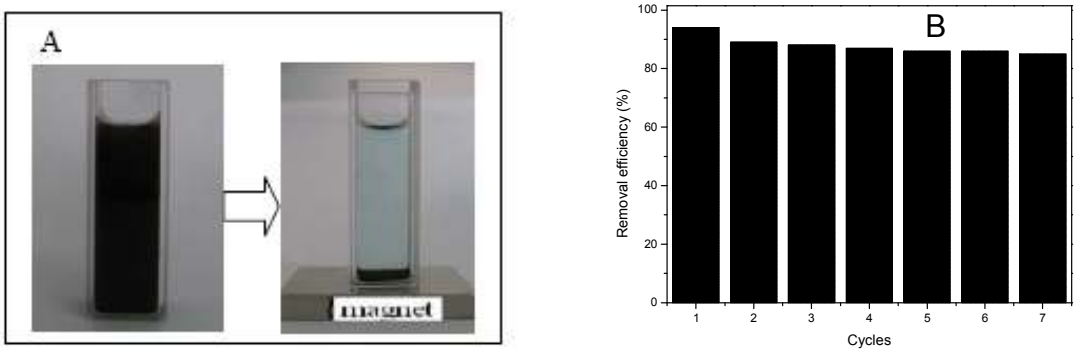

Figure 7 The separation of $NiFe_2O_4$ nanoparticles from solution by a magnet (A) and removal efficiencies of arsenic during adsorption-desorption cycles for $NiFe_2O_4$ nanoparticles (B)

The graph of removal efficiency of arsenic as a function of time for various amounts of the nanocomposite used are shown in Figure 8. 94% removal is observed within few minutes when 0.5 g/L of the nanocomposite is used for 25 mg/L arsenic solution. The amount adsorbed is calculated using the relation, qe = $(C_i - C_f)V$ /m, where C_i and C_f are the initial and final concentrations of arsenic, respectively, in mg/L, and m is mass of the nanoparticles in mg/L. The value of qe is calculated as 18 mg/g. Similar high adsorption capacity for drimaren red dye and other contaminants is reported for iron oxide/commercial AC composite [27]. qe of 11.9 mg/g of Fe_3O_4/carbon nanotube nanocomposite is reported very recently for methylene blue (MB) removal [28].

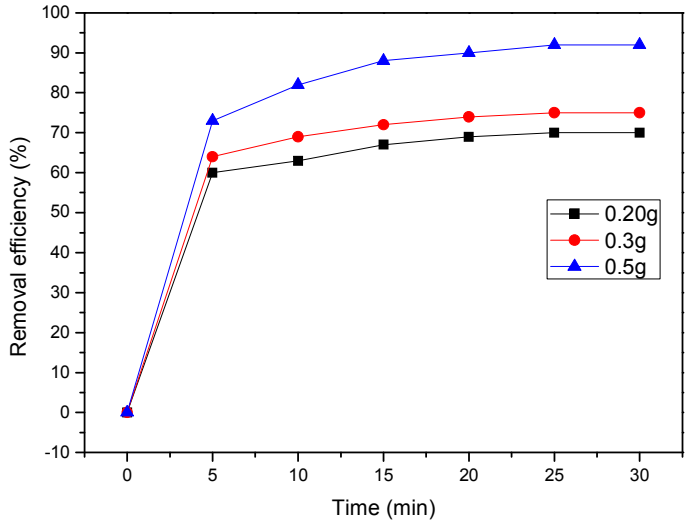

Figure 8 Removal efficiency of arcenic from water as a function of time using different amounts of $NiFe_2O_4$ nanoparticles.

Conclusion

Thus, the present study shows that superparamagnetic $NiFe_2O_4$ nanoparticles were successfully synthesized by using PEG assisted hydrothermal method and arsenic strongly attached to these nanoparticles. The magnetic fluid obtained by dispersion of the nanoparticles in water is relatively stable and this dispersion is very efficient for the removal of arsenic from contaminated water by adsorption on magnetic nanoparticles and a subsequent simple magnetic separation process. Also, these nanoparticles can be used repeatedly to remove arsenic from drinking water.

References

[1] H. Gleiter, Prog. Mater. Sci., 33 (1989) 223.

[2] C. Suryanarayana, Int. Mater. Rev., 40 (1995) R 41.

[3] Y. Köseoğlu, H. Kavas, J. Nanosci. Nanotechnol., 8 (2008) 584.

[4] Chin-Yih. Hong, I. J. Jang, H. E. Horng, C. J. Hsu, Y. D. Yao, and H. C. Yang, J. Appl. Phys. 81 (1997) 4275.

[5] R. N. Viswanath, S. Ramasamy, R. Ramamoorthy, P. Jeyavel, and T. Nagarajan, Nanostructured Mater., 6 (1995) 993.

[6] M. E. McHenry, M. A. Willard, and D. E. Laughlin, Prog. Mater. Sci., 44 (1999) 291.

[7] M. Sertkol, Y. Köseoğlu, A. Baykal, H. Kavas, A.C. Başaran, J. Magn. Magn. Mater. 321 (2009) 157.

[8] H. Kavas, A. Baykal, M. S. Toprak, Y. Köseoğlu, M. Sertkol, B. Aktas, Journal of Alloys and Compounds 479 (2009) 49–55.

[9] D. C. Jiles, Acta Mater., 51 (2003) 5907.

[10] Q. A. Pankhurst, J. Connolly, S. K. Jones, and J. Dobson, J. Phys. D: Appl. Phys., 36 (2003) R167.
[11] M. Grätzel, Nature 414 (2001) 338.

[12] T. Mütschele and R. Kirchheim, Scripta Metall., 21 (1987) 1101.

[13] Y. M. Slokar and A. M. Le Marechal, *Dyes Pigments,* 37 (1998) 335.

[14] R. T. Nickson, J. M. McArthur, P. Ravenscroft, W. G. Burgess, and K. M. Ahmed, *Appl. Geochem.,* 15 (2000) 403.
[15] S. Dixit and J. G. Hering, *Environ. Sci. Technol.,* 37 (2003) 4182.

[16] L. C. Roberts, S. J. Hug, T. Ruettimann, M. M. Billah, A. W. Khan, and M. T. Rahman, *Environ. Sci. Technol.,* 38 (2004) 307.

[17] C. T. Yavuz, J. T. Mayo, W. W. Yu, A. Prakash, J. C. Falkner, S. Yean, L. Cong, H. J. Shipley, A. Kan, M. Tomson, D. Natelson, and V. L. Colvin, *Science,* 314 (2006) 964.

[18] M. Sertkol, Y. Köseoğlu, A. Baykal, H. Kavas, A. Bozkurt, M.S. Toprak, Journal of Alloys and Compounds, 486 (2009) 325–329.

[19] M.R. Anantharaman, S. Jagatheesan, S. Sindhu, K.A. Malini, A. Narayanasamy, C.N. Chinnasamy, K. Philip, K. Vasudevan, Int. J. Plast. Rubb. Process. Appl. 27 (1998) 77–81.

[20] M.G. Buerger, Crystal Structure Analysis, Wiley interscience, New York, 1960.

[21] H. Ohnishi, T. Teranishi, J.Phys. Soc Jpn, 6 (1969) 36.

[22] S.Singhal, K.Chandra, Jour. Sol. Stat. Chem. , 180 (2007) 296-300.

[23] Wohlfarth, Ferromagnetic materials Vol 3 North holland Publishing Company 1982 p196.

[24] Qiang-min Wei, Jian-bao Li, Yong-jun Chen, Yong-shen Han, Material Chemistry and Physics, 74 (2002), 340-343.

[25] F. Li, H.Wang, L.Wang, J.Wang, J. Magn. Magn. Mater., 309 (2007), 295.

[26] R.N. Bhowmik, R. Ranganathan, J. Magn. Magn. Mater., 248 (2002), 101.

[27] L. C. A. Oliveira, R. V. R. A. Rios, J. D. Fabris, V. Garg, K. Sapag, and R. M. Lago, *Carbon* 40 (2002) 2177

[28] J.-L. Gong, B. Wang, G.-M. Zenga, C.-P. Yang, C.-G. Niu, Q.-Y. Niu, W.-J. Zhou, and Y. Liang, *J. Hazardous Mater.* 164 (2009) 1517